Astron. Astrophys. 319, 630–636 (1997)

ASTRONOMY AND ASTROPHYSICS

Abundance analysis of roAp stars

II. HD 203932⋆

M. Gelbmann[1], **F. Kupka**[1], **W.W. Weiss**[1], **and G. Mathys**[2]

[1] Inst. of Astronomy, Univ. Vienna, Türkenschanzstr. 17, A-1180 Vienna, Austria (last_name@galileo.ast.univie.ac.at)
[2] European Southern Observatory, Santiago, Chile

Received 3 May 1996 / Accepted 20 August 1996

Abstract. A new tool to simplify abundance analyses which is based on stand-alone programs has been applied to the rapidly oscillating Ap star HD 203932 (BI Mic, CD −30° 18600, SAO 212996; Ap(SrEu), $V = 8.82$ mag). The spectroscopically determined $T_{\rm eff} = 7450 \pm 100$ K and $\log g = 4.3 \pm 0.15$ put this star close to the ZAMS. Other fundamental atmospheric parameters are $v_{\rm micro} < 0.6$ km s^{-1} and the total abundance of all iron peak elements [M/H] = 0.0±0.1.

The fundamental parameters put HD 203932 in a region of the HR-diagram where convection starts becoming efficient and the standard mixing length theory models lead to severe problems in the determination of the atmospheric parameters. The difference between the upper limit for $\log g$ obtained from several variants of the mixing length theory and the Canuto-Mazzitelli model indicates that the choice of a particular convection model can influence the determination of basic stellar parameters.

For the first time abundances were determined for HD 203932 showing a pattern for the 35 investigated elements which is similar to α Cir (Kupka et al. 1996, Paper I). Fe and Ni have about solar abundance, Cr and especially Co are clearly overabundant as well as rare earth elements. The most underabundant element is Sc, followed by C, N, and O, which is a common property of CP2 stars. The lack of a correlation in our data between individual line abundances and their effective Landé factors implies a mean magnetic field modulus not exceeding few kG.

Compared to the last homogeneous spectroscopic investigation of a large sample of chemically peculiar stars (21 cool Ap stars, Adelman 1973), our analysis is based on data with higher spectral resolution *and* signal-to-noise ratio. Even more important, we are using a much larger atomic line data base with more precise atomic parameters than available more than twenty years ago.

Key words: stars: abundances; atmospheres; chemically peculiar; magnetic fields; oscillations; HD 203932

1. Introduction

Rapidly oscillating Ap (roAp) stars are a subgroup of the CP2 stars (chemically peculiar stars with a global magnetic field), which oscillate with frequencies from 0.9 to 4.8 mHz. The oscillations of roAp stars are non-radial, high overtone, low order (ℓ) acoustic p-modes with the axis of oscillation aligned to the axis of the magnetic field (Kurtz 1982). Their photometric amplitudes range up to 16 mmag and their effective temperatures from 7000 K to 8500 K. Reviews on rapidly oscillating Ap stars can be found in Shibahashi & Saio (1985), Weiss (1986), Shibahashi (1987), Kurtz (1986, 1990), and Matthews (1991).

The main purpose of our project is to provide accurate fundamental parameters like $T_{\rm eff}$, $\log g$ and abundances for pulsating chemically peculiar stars. In context of asteroseismology, these parameters serve as important boundary values for pulsation models, which are needed to determine the internal structure of these stars. This paper is the second one in a series on spectral analyses of roAp stars. Paper I deals with α Cir, the brightest member of the group of roAp stars (Kupka et al. 1996), and comments in detail on the significance and astrophysical motivation of our spectroscopic investigation of roAp stars.

HD 203932 (BI Mic, CD −30° 18600, SAO 212996) is classified as an Ap(SrEu) star (Bidelman & MacConnell 1973; Houk 1982) with $V = 8.82$ mag. Kurtz (1984) discovered the pulsation of HD 203932. It pulsates with a dominating frequency of 2.805 mHz and with a peak-to-peak amplitude of 0.66 mmag. The star has an Hβ index of $\beta = 2.791$ and Strömgren indices of $b - y = 0.169$, $m_1 = 0.196$ and $c_1 = 0.736$ (Vogt & Faundez 1979).

Send offprint requests to: Michael Gelbmann

⋆ Based on observations obtained at the European Southern Observatory (La Silla, Chile)

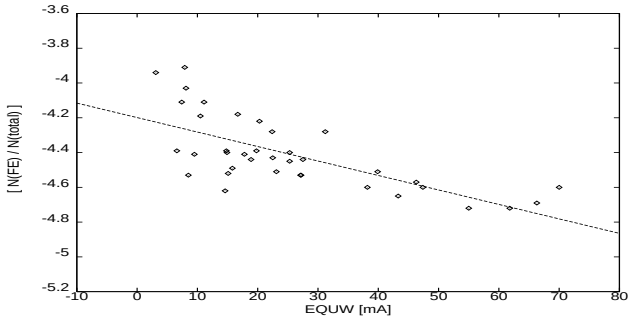

Fig. 1. Iron 'line' abundances plotted versus the equivalent widths, based on a model atmosphere with $v_{\rm micro}$ of 2 km s^{-1} which is too large (for comparison see Fig. 6). The dashed line is a linear least squares fit.

2. Observations

Two echelle spectra were obtained by G. Mathys at the European Southern Observatory in June 1992 with the ESO Multi Mode Instrument mounted on the New Technology Telescope. The Red Medium Dispersion spectroscopy mode was used in combination with the CCD #18 (Thomson 1024x1024 pixels). The echelle grating #10 with two different cross-disperser grisms covered the entire spectral range from 4200 to 8100 Å. Grism #6 allows to observe 22 well separated orders in a wavelength range from 6200 to 8100 Å. Grism #5 covers 46 orders, ranging from 4200 to 6400 Å. The spectral range of each order varies from 40 to 90 Å for the blue exposure, and from 90 to 120 Å for the red exposure. The spectral resolution in the blue region is R = 23000, and R = 25000 in the red.

The typical signal-to-noise ratio per pixel is about 200 in the continuum. To avoid the influence of the decreased signal-to-noise ratio far from the blaze, each order was trimmed such that two consecutive orders overlap only by approximately 10 to 20 Å.

Echelle spectra of A-type stars pose the well-known problem of defining the continuum in the relatively large spectral interval which is covered by hydrogen line wings. Echelle orders adjacent to those which contain the hydrogen lines were therefore interpolated to determine the trend in the blaze function and continuum.

All reductions of the observations to one continuous spectrum and the normalization to the continuum were done within the echelle package of IRAF. The normalization to the continuum was independently checked and confirmed by T. Ryabchikova using PC-IPS (Piskunov & Smirnov 1994).

3. AAP – abundance analysis procedure

The program AAP is a new tool which was developed for an easy, largely automatic and user friendly abundance analysis. In its present version AAP uses model atmospheres with scaled solar abundances, based on precalculated opacity distribution functions. A description of AAP, including a user's manual, is given in Gelbmann (1995).

Table 1. The final atmospheric parameters of HD 203932, based on a MLT model atmosphere, derived from 16 unblended iron lines and with error estimates.

Parameter	Value	Error Range
$T_{\rm eff}$	7450 K	7350...7550 K
$\log g$	4.3	4.15...4.45
[M/H]	0.0	-0.1...+0.1
$v_{\rm micro}$	0.0 km s^{-1}	0.0...0.6 km s^{-1}
$v \cdot \sin i$	12.5 km s^{-1}	10.0...15 km s^{-1}

The procedure makes use of the Vienna Atomic Line Database VALD (Piskunov et al. 1995), to compile spectral line lists of selected or all chemical elements. VALD is a set of critically evaluated lists of astrophysically important atomic transition parameters and includes supporting extraction software.

The main menu items of AAP are:

Calculate model atmosphere: computes atmospheres with chosen effective temperature, surface gravity, metallicity, and microturbulent velocity.

Select wavelength range: defines the desired wavelength range and starts PRESELECT and SELECT, written by Kupka and Piskunov.

PRESELECT scans through all line lists of VALD and creates an output table which contains the wavelength, the Kurucz-code of the element with ionization stage, the gf-value, the lower and upper energy level, the effective Landé-factor, and the three line broadening constants for each line found. This list contains all data needed by AAP to calculate synthetic spectra in the given wavelength region.

SELECT calculates the core depths for all lines in the preselected list and selects only those lines which contribute significantly to the synthetic spectrum. Spectral lines with a line depth smaller than a chosen limit are rejected.

Generate line list: creates a subset of the previously selected line list of a *particular* chemical element in a given wavelength range. Blended lines with a chosen ratio in line depth of the components (typically more than 30%) within a chosen interval (typically 0.3Å) are rejected. In addition it is possible to eliminate all spectral lines which are in critical wavelength regions like the wings of the Hydrogen Balmer lines or close to telluric lines. Hence, only those lines which are considered to be sufficiently free from blends are included in this subset.

Synthesize lines: calculates a synthetic spectrum with SYNTH and ROTATE, written by Piskunov (1992), and takes into account various broadening mechanisms. Either all spectral lines of all chemical elements in a chosen wavelength range are used, or all spectral lines of a line list of a particular chemical element. To compute Balmer profiles the program BALMER9 (Kurucz 1993) is used.

It is possible to fit automatically an unblended synthetic spectral line to an observed line. This autofit algorithm minimizes the difference between the observed and the synthetic

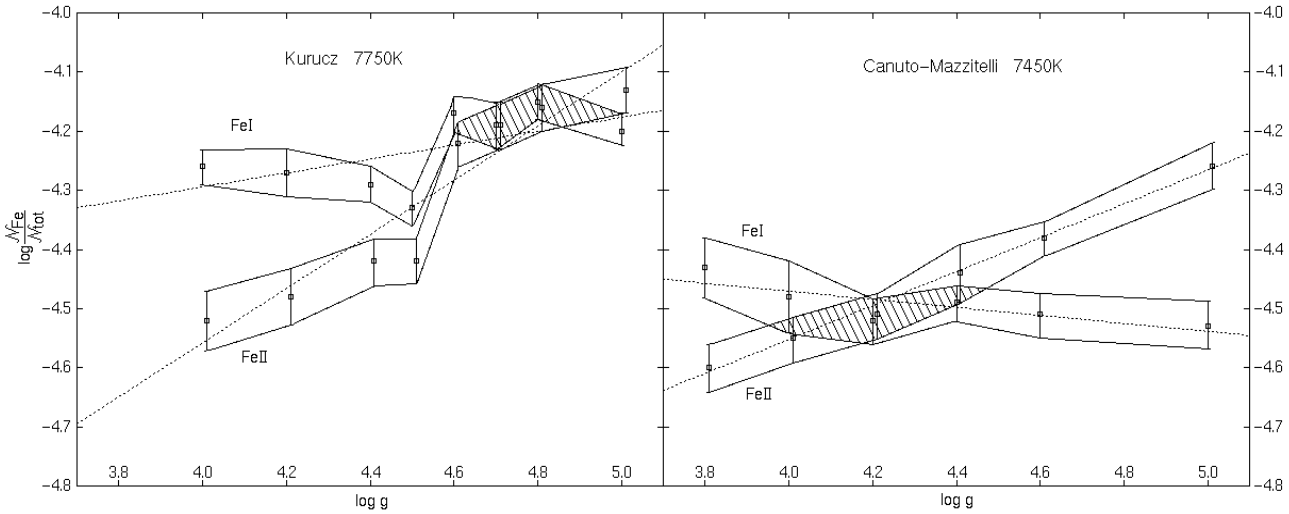

Fig. 2. Abundances of neutral and single ionized iron as a function of $\log g$ for different convection models. The error bars are standard deviations from the mean, and the dotted lines are linear least square solutions. $T_{\rm eff}$ and $\log g$ values in the hatched areas are formal solutions which fit all the observed iron lines equally well. Left: Kurucz ATLAS9 model atmosphere with standard mixing length theory. See text for comments on the kink at $\log g = 4.55$. Right: Kurucz ATLAS9 model atmosphere with the Canuto-Mazzitelli convection model.

spectrum, i.e. the area between the two spectra, with the method of the golden section search (Press et al. 1986). The free parameter for this minimization is the element abundance. Hence, an accepted fit of a synthetic line to the observations gives a 'line' abundance for a chosen atmosphere (see Fig. 4). The final element abundance results as a mean from individual fits to all unblended spectral lines of that element.

Plot abundances: produces diagrams of 'line' abundances versus atomic line parameters for a given chemical element. Since different atomic line parameters are sensitive to different stellar parameters, it is possible to check the consistency of the chosen atmospheric parameters. If no trends are found between 'line' abundances and the equivalent widths (primarily sensitive to $v_{\rm micro}$), the lower energy levels ($T_{\rm eff}$), the ionization stages ($\log g$), and the effective Landé factors (magnetic field), the chosen atmosphere is assumed to be correct. A more detailed description of the explained method is given in Wehrse (1988), especially with respect to the achievable accuracies (systematic errors) and with more detailed considerations on secondary dependencies of atomic line parameters on various stellar parameters. An example of such an analysis based on an incorrectly chosen microturbulent velocity is given in Fig. 1. Diagrams for the finally adopted atmospheric parameters are shown in Figs. 5 and 6 (different scale!).

4. Model atmosphere

The starting model atmosphere parameters for the star HD 203932, derived from synthetic Strömgren indices based on Kurucz' model atmospheres, were $T_{\rm eff} = 7750$ K, $\log g = 4.5$, and metallicity [M/H] = 0.1, with an estimated microturbulent velocity of $v_{\rm micro} = 2.0$ km s^{-1}. Although the suggested $\log g$ value was too large, we followed this standard procedure in the expectation that subsequent iterations finally would result in an astrophysically consistent $\log g$. However, after several iterations of ATLAS9 model atmospheres (Kurucz 1993), a formal solution was found with an even larger $\log g = 4.6$, hence putting HD 203932 below the ZAMS. Theories and observations indicate a $\log g = 4.35$ for a star at the ZAMS with comparable $T_{\rm eff}$ (Andersen 1993). This discrepancy led us to investigate in more detail the $T_{\rm eff}$ - $\log g$ parameter space for which the criteria for a consistent spectrum analysis are fulfilled (no trends in 'line' abundances, see *Plot abundances* in Sect. 3).

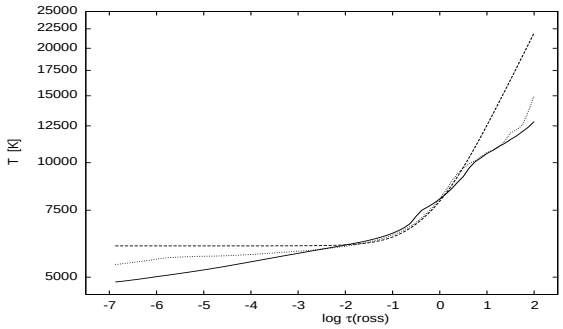

Fig. 3. Temperature versus the Rosseland optical depth (on a logarithmic scale) of the model atmosphere used for HD 203932. The starting model (dashed line) changes after four iterations to the model represented by the dotted line. After 95 iterations all temperature corrections were smaller than one percent, all flux and flux derivative errors negligible. This converged model (solid curve) was used for the final analysis.

The technique used to determine $\log g$ assumes ionization equilibrium and depends on both neutral and ionized stages.

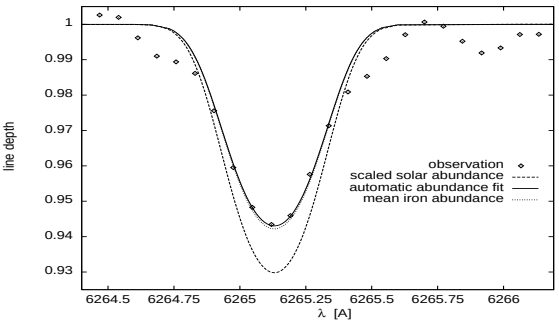

Fig. 4. Fe I line at 6265.131 Å: The synthetic spectral lines computed for a scaled solar atmosphere with [M/H] = 0.1 and for the finally adopted mean iron abundance are compared with our observations. The automatic abundance fit, resulting in an individual 'line' abundance, is the best representation of the observations.

The most abundant iron ion in the temperature range of interest is Fe II, whereas Fe I contributes less than 1%. Our analysis was performed with 10 Fe I and 6 Fe II carefully selected lines which are unblended, well defined and have accurately known gf-values. Fig. 2 illustrates how the abundances for neutral and single ionized iron depends on $\log g$. Based on the analysis of other elements with sufficient number of lines observable in the spectrum, NLTE effects, as are discussed by Gigas (1986) for Vega, seem to be negligible and do not account for different $\log g$ values for different ionization stages.

Considering the abundance errors and the different sensitivity for different ions on $\log g$, one expects a rhombus-shaped area of intersection, which obviously is not the case for the ATLAS9 models used so far (Fig. 2-left). There is a clear kink at $\log g = 4.55$ (and $T_{\rm eff} = 7750$ K) which coincides with regions in the calibration of Strömgren colors (Kupka 1996, Smalley 1996), where severe problems due to modeling convection and overshooting in ATLAS9 are known. We therefore repeated our analysis with model atmospheres with different treatment of convection, based on classical mixing length theory: ATLAS9 as is published by Kurucz on CD-ROMs (1993), the same model atmospheres, but without overshooting, and ATLAS9 with flux smoothing (Castelli 1996). For comparison, we also used a non-MLT version of ATLAS9, based on a convection model according to Canuto & Mazzitelli (1991).

Indeed, all improved ATLAS9 models avoid the discontinuity as is shown in Fig. 2-left. However, we were faced with the fact that for a rather large interval of $T_{\rm eff}$ and $\log g$ formal solutions with comparable internal errors for the iron abundance are possible. The hottest MLT models with a formal solution have $T_{\rm eff} = 7600$ K and $\log g = 4.6$, whereas the CM formalism gives $T_{\rm eff} = 7450$ K and $\log g = 4.3$ (Fig. 2-right). The cool limit for the same type of models is beyond $T_{\rm eff} = 7000$ K and $\log g = 3.5$ and was not explicitly determined by us. We had to use the temperature dependency of the Balmer hydrogen lines to reduce this large temperature interval which allows formally equivalent solutions.

Hα, Hβ, and Hγ lines are available for a comparison of observed and synthetic BALMER9 profiles. Despite the already explained difficulties with normalization to the continuum of echelle spectra in the region of hydrogen lines, we were able to clearly define temperature limits beyond which the observations could not be fitted by synthetic profiles any more.

These limits are for Hα: $T_{\rm eff} = 7250$ K to 7500 K, for Hβ: $T_{\rm eff} = 7300$ K to 7600 K, and for Hγ: $T_{\rm eff} = 7300$ K to 7600 K. Hence, the lower temperature limit for model atmospheres for HD 203932 can be set to $T_{\rm eff} = 7300$ K.

This lower limit, together with the upper limits derived from the analysis of iron results in astrophysically relevant formal solutions for MLT based models: $T_{\rm eff} = 7300$ K to 7600 K with $\log g = 4.0$ to 4.6, and for CM based models: $T_{\rm eff} = 7300$ K to 7450 K with $\log g = 4.0$ to 4.3.

The final model atmosphere parameters, which were used to estimate the abundances for all measurable chemical elements of HD 203932, are given in Table 1. They are determined from the mean MLT model, corresponding also to the hottest possible CM model. Fig. 3 shows the temperature gradient of the converged model atmosphere used for the abundance analysis.

In order to be consistent with earlier analyses of (ro)Ap stars, we decided to continue with MLT based model atmospheres. This consistency is important for the detection of abundance pattern which might allow to distinguish the group of roAp stars from others. We have indications that the abundance *pattern* derived from MLT and CM models are similar, but only slightly scaled.

The standard photometric calibration based on chemically *normal* stars (Rogers 1995, and references therein) gives $T_{\rm eff} = 7620$ K, $\log g = 4.3$, [M/H] = 0.1 for the Strömgren system (Crawford 1979), and $T_{\rm eff} = 7480$ K, $\log g = 4.3$, [M/H] = 0.1 for the Geneva system (Künzli et al. 1996). These values are in good agreement with our spectroscopically determined parameters.

For the microturbulent velocity an upper limit of $v_{\rm micro} = 0.6$ km s^{-1} was determined, but to avoid interpolations in the grid of opacity distribution functions $v_{\rm micro} = 0.0$ km s^{-1} was used. Anyhow, the abundances are insensitive to such small differences in $v_{\rm micro}$.

The value for $v \cdot \sin i = 12.5$ was determined with ROTATE (Piskunov 1992), which allows a comparison of synthetic spectra convolved with kernels representing various broadening mechanisms with observations.

No indication for a measurable magnetic field was found by the visual inspection of the spectra. Also, no correlation exists between the abundances derived from individual lines and their effective Landé factors. A linear least squares fit results in a slope of $+0.01 \pm 0.05$ for 'line' abundances versus $\overline{g}_{\rm eff}$. This is consistent with the absence of detection of a magnetic field in HD 203932 in two attempts made by Mathys & Hubrig (1996, in preparation).

5. Fine analysis of HD 203932

All calculations used for the present abundance analysis for HD 203932 have been performed by using the Abundance Analysis Procedure AAP (see Sect. 3) and are based on the model atmosphere given in Table 1.

Table 2. Abundances of elements normalized to the total number of atoms with error estimates in units of 0.01 dex, for the roAp star HD 203932 and for the sun. The number of lines used in our analysis is given separately for the neutral and the single ionized element. The column $[\mathcal{N}]$ gives the logarithmic ratio of elements relative to the sun.

Element	$\log\left(\frac{\mathcal{N}}{\mathcal{N}_{\rm tot}}\right)_{\rm HD}$	No.of lines I / II	$[\mathcal{N}]$	$\log\left(\frac{\mathcal{N}}{\mathcal{N}_{\rm tot}}\right)_{\odot}$
C	−4.09(30)	9/0	−0.61	−3.48
N	−4.40(21)	2/0	−0.41	−3.99
O	−3.73(28)	7/0	−0.62	−3.11
Na	−5.72(38)	7/0	−0.01	−5.71
Mg	−4.23(15)	10/5	+0.23	−4.46
Al	−5.34(13)	7/0	+0.23	−5.57
Si	−4.39(38)	50/6	+0.10	−4.49
S	−5.05(12)	10/0	−0.22	−4.83
Cl	−6.54(50)	1/0	0.00	−6.54
K	−6.81(26)	2/0	+0.11	−6.92
Ca	−5.17(25)	24/3	+0.51	−5.68
Sc	−9.77(30)	0/3	−0.83	−8.94
Ti	−7.01(27)	5/17	+0.04	−7.05
V	−7.49(20)	4/0	+0.55	−8.04
Cr	−5.64(27)	24/10	+0.73	−6.37
Mn	−6.39(29)	10/0	+0.26	−6.65
Fe	−4.42(16)	41/28	−0.05	−4.37
Co	−5.97(15)	12/0	+1.15	−7.12
Ni	−5.88(15)	14/0	−0.09	−5.79
Cu	−7.89(37)	3/0	−0.06	−7.83
Zn	−7.88(19)	2/0	−0.44	−7.44
Sr	−7.38(50)	1/2	+1.76	−9.14
Y	−8.29(23)	0/21	+1.51	−9.80
Zr	−9.27(40)	0/4	+0.17	−9.44
Ba	−9.33(23)	0/5	+0.58	−9.91
La	−10.10(31)	0/4	+0.72	−10.82
Ce	−9.27(47)	0/15	+1.22	−10.49
Pr	−10.09(37)	0/3	+1.24	−11.33
Nd	−9.50(27)	0/18	+1.04	−10.54
Sm	−10.06(29)	0/5	+0.98	−11.04
Eu	−9.15(40)	0/8	+2.38	−11.53
Gd	−9.90(37)	0/4	+1.02	−10.92
Er	−9.73(50)	0/1	+1.38	−11.11
Lu	−10.40(21)	0/2	+0.88	−11.28
Th	−10.85(05)	0/2	+1.07	−11.92

After defining the fundamental stellar parameters, line lists for all chemical elements were generated with VALD. In the case of HD 203932 and the selected wavelength range of 4200 to 8100 Å, almost 100 000 spectral lines of many chemical elements were found. Almost 8000 spectral lines with a core depth exceeding one percent were kept for a further analysis which finally is based on 408 spectral lines, ignoring those in the Balmer wings and in spectral regions crowded with telluric lines.

The abundance of a particular chemical element for an individual spectral line was adjusted in such a way that the synthetic spectral line showed an optimum fit to the observed one (see Sect. 3). The mean abundance for a particular chemical element was determined by averaging all individual 'line' abundances.

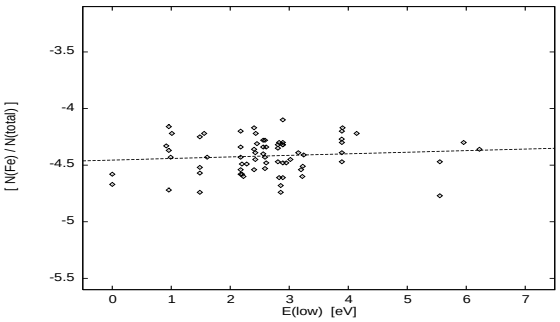

Fig. 5. Confirmation of the effective temperature of HD 203932: Abundances of 41 Fe I (diamonds) and 28 Fe II lines (crosses) are plotted versus the lower energy level for $T_{\rm eff} = 7450$ K.

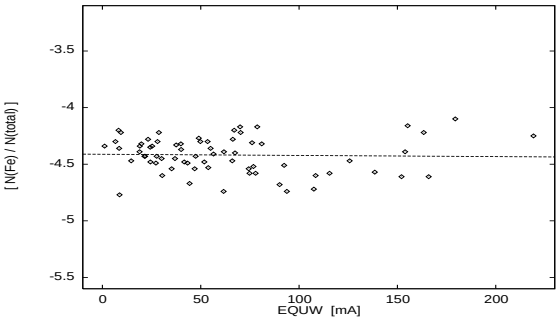

Fig. 6. Confirmation of the microturbulent velocity. Abundances versus equivalent width of 41 Fe I (diamonds) and 28 Fe II lines (crosses) are plotted for $v_{\rm micro} = 0.0$ km s^{-1}.

The same procedure was performed for as many elements as possible. Trend plots of all investigated elements (Fig. 5 and 6 show examples for iron) confirmed the atmospheric parameters given in Table 1.

Fig. 4 gives an example for the fitting procedure of the iron line at 6265.131 Å. The bullets represent the observed spectrum. The solid curve shows the optimum fit derived from the autofit algorithm for this individual iron line ($\log(\mathcal{N}_{\rm Fe}/\mathcal{N}_{\rm tot}) = -4.43$). The dashed curve shows the synthetic line for a scaled solar ([M/H] = 0.1) iron abundance ($\log(\mathcal{N}_{\rm Fe}/\mathcal{N}_{\rm tot}) = -4.27$), which represents the initial starting value for the autofit algorithm. Finally, the dotted curve shows the synthetic line with the mean iron abundance ($\log(\mathcal{N}_{\rm Fe}/\mathcal{N}_{\rm tot}) = -4.42$).

Fig. 5 confirms the chosen effective temperature of HD 203932. It shows the abundance values of 41 Fe I and 28 Fe II lines, estimated with the autofit algorithm, versus the lower energy level. Each data point represents the abundance of one synthetic iron line. The dashed line is a linear least squares fit for which the slope is 0.014 ± 0.016.

Fig. 6 confirms the chosen microturbulent velocity. It shows the abundances of the same 69 iron lines as in Fig. 5 versus their equivalent width.

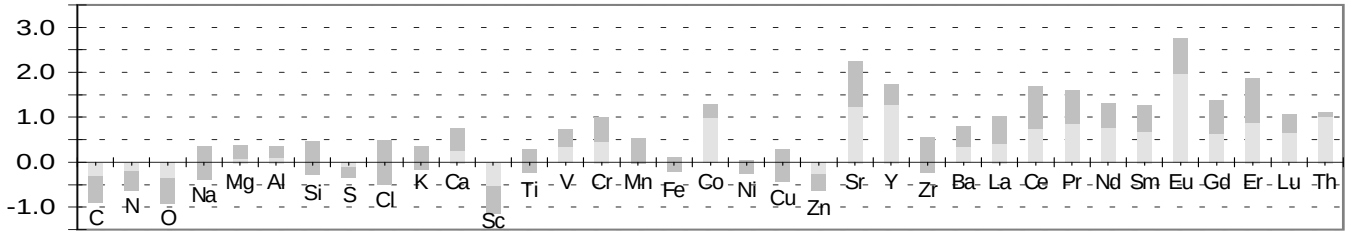

Fig. 7. Logarithm of abundances for HD 203932 relative to the sun with estimated error ranges indicated in dark grey.

6. Abundances

Table 2 summarizes the abundances of all investigated elements and compares them to results for the sun (Anders & Grevesse 1989). The quoted errors between brackets are standard deviations of the individual 'line' abundances to the mean. If only one line could be used, an error of ± 0.5 was estimated.

Fig. 7 shows the deviation from solar abundances for 35 elements in the atmosphere of HD 203932. This result is based on the analysis of more than 400 spectral lines.

6.1. Light elements

The underabundances of C, N and O, which seem to be typical for roAp stars, are confirmed. Na, Mg, Al, Si, S, Cl, and K have practically solar abundance. However, it has to be stressed that the results for Cl and K are uncertain, because only few unblended lines exist in the observed wavelength region. The deviations for Na and Si are large due to the uncertain oscillator strengths for many of their spectral lines.

6.2. Iron peak elements

The abundances of the iron peak elements Ti, Fe, and Ni are practically solar. Ca and Mn are slightly overabundant, V, Cr and especially Co are strongly overabundant. An exception is the element Sc, which is underabundant. The errors for the iron peak elements are relatively small, because of the large number of measured lines. A very interesting feature is the prominent overabundance of Co, which is similar to what we have found for α Cir (Paper I). Such a Co overabundance in magnetic Ap stars does not seem to be widespread. The best documented cases so far were the (significantly hotter) stars HD 22316 (Sadakane 1992) and HD 116458 (Dworetsky et al. 1980).

The total abundance of all iron peak elements available within this study results in a metallicity of [M/H] = 0.0 (see Sect. 4).

6.3. Rare earth elements and other heavy elements

All rare earth elements and the heavy elements Sr, Y, Zr, Ba, and Th are overabundant, which seems to be typical for CP2 stars. Cu and Zn abundances are close to the solar values, but may be uncertain due to the small number of usable lines.

The odd-even rule (an element with an odd atomic number is less abundant than its neighbours) seems to be slightly violated by the sequence Sr-Y-Zr and might be even strongly violated by the sequence Sm-Eu-Gd. It has to be mentioned that the Eu abundance was derived from eight lines which did not include the two most prominent Eu II lines (4205Å & 4435Å). These lines in the blue spectral region have the well known problem of hyperfine structure splitting which is not yet considered in our analysis. In the past, neglecting hyperfine structures has resulted in significantly overestimated abundances.

7. Conclusion

The determination of basic atmospheric parameters for HD 203932 has revealed that this roAp star is located in a region of the HR-diagram sensitive to the treatment of convection. The large error interval for $T_{\rm eff}$ obtained from iron lines had to be confined by a comparison of observed and computed Balmer line profiles. The difference between the upper limit for $\log g$ obtained from several variants of the mixing length theory and the CM model indicates that the choice of a particular convection model can have an influence on the determination of basic parameters derived from spectroscopy for cool (ro)Ap stars and probably also other stars with similar $T_{\rm eff}$ and $\log g$. HD 203932 might be a suitable test case for modeling convection in stellar atmospheres. Furthermore, the high $\log g$ value, putting HD 203932 close to the ZAMS, creates problems for the theory that CP2 stars have developed their peculiarity at the end of the main sequence life time (Hubrig & Schwan 1991).

In order to be consistent with earlier analyses of (ro)Ap stars, we decided to continue with MLT based model atmospheres. We have indications that the abundance *pattern* derived from MLT and CM models are similar, but only marginally scaled. A more detailed investigation of the problem of modeling convection and its effect on abundance determinations is needed for improving the accuracy of absolute abundances. Meanwhile, we can rely on relative abundance pattern.

The overall abundance pattern of HD 203932 is similar to that one of α Cir. Nevertheless, there are some notable differences for several of the other basic parameters. Although being cooler by about 500 K, the apparent microturbulence of HD 203932 is clearly smaller. Contrary to the case of α Cir we have found no indication for a magnetic field. Hence, convection should be more important for HD 203932 than for α Cir

which supports the choice of Kupka et al. (1996) to attribute a large fraction of the observed microturbulence to magnetic intensification.

For the present analysis Kurucz model atmosphere with scaled solar abundances have been used. Thus, we cannot expect that our procedure provides a self consistent solution for HD 203932 which clearly does not follow such a (scaled) solar abundance pattern (see Fig. 7). Presently, we are working on individualized opacity distribution function tables which shall allow us to eliminate this shortcoming by computing self consistent model atmospheres.

This analysis is based on spectra obtained at a particular rotation phase of HD 203932. No rotation period is published for this star, despite the fact that photometric surveys have resulted in the determination of rotation periods of other CP stars. No such variability is reported for HD 203932 which suggests a small light amplitude. Consequently, we are looking either close to the rotation pole, or the surface inhomogeneities which cause brightness modulation due to rotation, are small. In both cases, one can assume that abundance determinations are only marginally effected by rotation. Thus, the abundances determined in the present paper are probably representative for the entire visible atmosphere of HD 203932.

Acknowledgements. This research was done within the working group *Asteroseismology-AMS*. The calculations were performed with a DEC AXP-3000/600, funded through a DEC-EERP project (STARPULS). Research was supported by the FFwF (project *P 8776-AST*). T. Ryabchikova from the Astron. Inst. of the Russian Academy of Sciences contributed with many helpful discussions.

References

Adelman S.J., 1973, ApJ 183, 95
Anders E., Grevesse N., 1989, Geo. Cosmochim. Acta 53, 197
Andersen J., 1993, in: W.W. Weiss & A. Baglin (eds.), Inside the Stars, ASP Conf. Ser., Vol. 40, p. 347
Bidelman W.P., MacConnell D.J., 1973, AJ 78, 687
Canuto V.M. & Mazzitelli I., 1991, ApJ 370, 295
Castelli F., 1996, in S. Adelman, F. Kupka, W.W. Weiss (eds.), Workshop on Model Atmospheres and Spectral Synthesis, ASP Conf. Ser., in press
Crawford D.L., 1979, AJ 84, 1858
Dworetsky M.M., Trueman M.R.G., Stickland D.J., 1980, A&A 85, 138
Gelbmann M., 1995, Comm. Asteroseismology 89
Gigas, D., 1986, A&A 165, 170
Houk N., 1982, Michigan Spectral Catalogue, Vol. 3, Department of Astronomy, University of Michigan, Ann Arbor
Hubrig S., Schwan H., 1991, A&A 251, 469
Künzli M., North P., Kurucz, R.L., Nicolet B., 1996, A&AS, in press
Kupka F., 1996, in: S. Adelman, F. Kupka, W.W. Weiss (eds.), Workshop on Model Atmospheres and Spectral Synthesis, ASP Conf. Ser., in press
Kupka F., Gelbmann M., Heiter U., Kuschnig R., Weiss W.W., Ryabchikova T.A., 1995, in: R.S. Stobie, P.A. Whitelock (eds.), Astrophysical Applications of Stellar Pulsation, ASP Conf. Ser., Vol. 83, p. 317
Kupka F., Ryabchikova T.A., Weiss W.W., Kuschnig R., Rogl J., Mathys G., 1996, A&A 308, 886
Kurtz D.W., 1982, MNRAS 200, 807
Kurtz D.W., 1984, MNRAS 209, 841
Kurtz D.W., 1986, in: D.O. Gough (ed.), Seismology of the Sun and Distant Stars, Proc. NATO Workshop, Reidel, p.417
Kurtz D.W., 1990, ARA&A 28, 607
Kurucz R.L., 1993, CDROM13, SAO Cambridge
Matthews J.M., 1991, PASP 103, 5
Mathys G., Hubrig S., 1996, in preparation
Piskunov N.E., Kupka F., Ryabchikova T.A., Weiss W.W., Jeffery C.S., 1995, A&AS 112, 525
Piskunov N.E., 1992, in: Y.V. Glagolevskij, I.I. Romanyuk, (eds.), Stellar magnetism, Nauka, St.Petersburg, p. 92
Piskunov, N.E., Smirnov, O.M., 1994, in: D.R. Crabtree, R.J. Hanisch, J. Barnes (eds.), Astronomical Data Analysis Software and Systems III, ASP Conf. Ser., Vol. 61, p. 245
Press W.H., Teukolsky S.A., Vetterling W.T., Flannery B.P., 1986, Numerical Recipes, Cambridge Univ. Press, p. 387
Rogers N.Y., 1995, Comm. Asteroseismology 78
Sadakane K., 1992, PASJ 44, 125
Shibahashi H., Saio H., 1985, PASJ 37, 245
Shibahashi H., 1987, Lect. Notes Phys. 274, 112
Smalley B., 1996, in: S. Adelman, F. Kupka, W.W. Weiss (eds.), Workshop on Model Atmospheres and Spectral Synthesis, ASP Conf. Ser., in press
Vogt N., Faundez M., 1979, A&AS 36, 477
Wehrse R. (ed.), 1988, Accuracy of Element Abundances from Stellar Atmospheres, Lect. Notes Phys. 365
Weiss W.W., 1986, in: C.R. Cowley, M.M. Dworetsky, C. Megessier (eds.), Upper Main Sequence Stars with Anomalous Abundances, IAU Coll. 90, Aph. Space Sc. Lib. Vol. 125, p. 219

This article was processed by the author using Springer-Verlag LaTeX A&A style file *L-AA* version 3.